Molecular mechanisms of the interhead coordination by interhead tension in cytoplasmic dyneins

Qian Wang[a], Biman Jana[b], Michael R. Diehl[c,d], Margaret S. Cheung[a,e], Anatoly B. Kolomeisky[a,c,d], and José N. Onuchic[a,d,f,g,1]

[a]Center for Theoretical Biological Physics, Rice University, Houston, TX 77005; [b]Department of Physical Chemistry, Indian Association for the Cultivation of Science, Jadavpur, 700032 Kolkata, India; [c]Department of Bioengineering, Rice University, Houston, TX 77030; [d]Department of Chemistry, Rice University, Houston, TX 77030; [e]Department of Physics, University of Houston, Houston, TX 77204; [f]Department of Physics and Astronomy, Rice University, Houston, TX 77005; and [g]Department of Biosciences, Rice University, Houston, TX 77005

Edited by Susan Marqusee, University of California, Berkeley, CA, and approved August 21, 2018 (received for review April 19, 2018)

Cytoplasmic dyneins play a major role in retrograde cellular transport by moving vesicles and organelles along microtubule filaments. Dyneins are multidomain motor proteins with two heads that coordinate their motion via their interhead tension. Compared with the leading head, the trailing head has a higher detachment rate from microtubules, facilitating the movement. However, the molecular mechanism of such coordination is unknown. To elucidate this mechanism, we performed molecular dynamics simulations on a cytoplasmic dynein with a structure-based coarse-grained model that probes the effect of the interhead tension on the structure. The tension creates a torque that influences the head rotating about its stalk. The conformation of the stalk switches from the α registry to the β registry during the rotation, weakening the binding affinity to microtubules. The directions of the tension and the torque of the leading head are opposite to those of the trailing head, breaking the structural symmetry between the heads. The leading head transitions less often to the β registry than the trailing head. The former thus has a greater binding affinity to the microtubule than the latter. We measured the moment arm of the torque from a dynein structure in the simulations to develop a phenomenological model that captures the influence of the head rotating about its stalk on the differential detachment rates of the two heads. Our study provides a consistent molecular picture for interhead coordination via interhead tension.

cytoplasmic dynein | molecular simulation | interhead coordination | interhead tension

The successful functioning of living systems strongly depends on the activities of several classes of enzymatic molecules, which are known as motor proteins or biological molecular motors (1–3). One of the most important motor proteins is cytoplasmic dynein, which is responsible for retrograde transport along microtubules (MTs) (4, 5). A dynein molecule can walk with a cellular cargo for hundreds of steps, that is, highly processively, before detaching from an MT (6, 7).

Cytoplasmic dynein is a large protein complex composed of two identical heavy chains and several other subunits. Each heavy chain includes a nonmotor tail domain and a motor head domain composed of a ring of six AAA+ domains, a stalk, and an MT-binding domain (MTBD) (8). One head is referred to as the "leading head" and the other is the "trailing head." Although the structural topology of dynein is similar to that of several other widely investigated motor proteins, such as kinesins and myosins V and VI (9, 10), the mechanism underlying their movement is different. Previous studies have shown that both kinesin and myosin molecules walk in a so-called hand-over-hand fashion (11, 12), indicating that for each step the leading head binds to the cytoskeletal filament while the trailing head detaches from the filament and swings from the back to the front. This rule does not depend on interhead separation. Surprisingly, the coordination between the two heads of a cytoplasmic dynein depends on the separation and the tension between the heads—the greater the separation, the higher the interhead tension. When the separation is small, the leading and trailing heads of cytoplasmic dynein have a similar probability of detaching from the MT and of stepping forward without apparent coordination (13, 14). When the leading head steps forward, the separation naturally increases. There is a backward tension on the leading head and a forward tension on the trailing head (Fig. 1*B*). The interhead tension differentially impacts the detachment rates of the two heads from the MTs. Both theoretical investigations (15) and single-molecule experiments (16, 17) have shown that the interhead tension accelerates the detachment rate of the trailing head from the MT but does not change the detachment rate of the leading head. Thus, the trailing head detaches and steps forward while the leading head remains on the MT. The tension has been speculated to alter the angle between the stalk of the cytoplasmic dynein and the MT (8). In addition, a previous study suggested that tension changes the bending direction of the stalk, thus affecting the detachment rate (18). These studies focused mainly on the flexible stalk of dynein (19, 20) that rotates about the principal axis of the MT or the axis perpendicular to the MT (x and y axes, respectively, in Fig. 1*A*). The role of the ring in transmitting the tension and breaking the symmetry of motion between the two heads remains unclear.

A major challenge of interrogating the effect of the interhead tension on the differential detachment rates of cytoplasmic dynein is the lack of a high-resolution structure of double-headed

Significance

Cell physiology strongly depends on motor proteins to transport and regulate the intracellular distributions of key materials and organelles. Cytoplasmic dynein, one of the most important biological motors in living cells, is an efficient retrograde motor due to its ability to step continuously along microtubule filaments. Dynein has two identical domains that are coordinated by interhead tension. However, the molecular mechanism of this coordination is not understood. By combining computer simulations with analytical calculations, we show that the interhead tension creates opposite torques on the leading and trailing heads, crucial for the coordination between the heads. Our finding provides a molecular basis for understanding the functionality of cytoplasmic dynein.

Author contributions: Q.W., M.S.C., A.B.K., and J.N.O. designed research; Q.W. performed research; Q.W., B.J., M.R.D., M.S.C., A.B.K., and J.N.O. analyzed data; and Q.W., B.J., M.R.D., M.S.C., A.B.K., and J.N.O. wrote the paper.

The authors declare no conflict of interest.

This article is a PNAS Direct Submission.

[1]To whom correspondence should be addressed. Email: jonuchic@rice.edu.

This article contains supporting information online at www.pnas.org/lookup/suppl/doi:10.1073/pnas.1806688115/-/DCSupplemental.

Published online September 17, 2018.

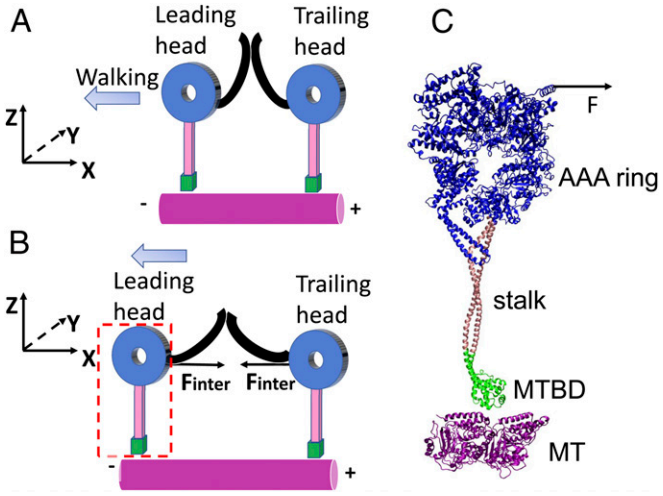

Fig. 1. Illustration of the studying system. (*A*) Double-headed cytoplasmic dynein docking on an MT. The blue arrow shows the walking direction of the dynein. (*B*) After the leading head steps forward, the distance between the leading and trailing heads increases, resulting in the interhead tension F_{inter}. The red box shows a single head, which is the region simulated in this study. (*C*) Structure of the single head, which includes an AAA ring (blue), a coiled-coil stalk (pink), and an MTBD (green). The head docks on a short MT (purple). An external force of 2 pN is applied to the N terminus of the single head (residue 1255Q in the crystal structure with Protein Data Bank ID code 4rh7) to mimic the interhead tension within a double-headed cytoplasmic dynein.

dynein. Even if a structure was available, the computational cost of an all-atom molecular dynamics simulation is prohibitively expensive. We therefore developed a strategy to overcome these challenges by using only one head as a modeling framework and by using coarse-grained molecular simulations. Because the two heads are structurally identical, we simply applied a force to one head in either direction pointing toward the plus or the minus end of the MT as a modeling framework for interrogating the effect of interhead tension on a double-headed dynein. We applied an external force on the N terminus positioned close to the hexameric ring (Fig. 1*C*). The head pulled by the force toward the minus end represents the trailing head, and the one pulled toward the plus end represents the leading head.

We built a molecular structure of a single head of dynein including a ring of six AAA+ domains, a stalk, and the MTBD that dock on an MT (Fig. 1*C*) from several crystal structures of fragmented dyneins (21–24). We employed a structure-based model (SBM) to probe the conformational transition of a dynein head driven by a force. Although the SBM neglects the energetic roughness that is typically present in all-atom simulations (25), the SBM has been useful in capturing key features of motions from motor proteins (26–29). Indeed, our SBM simulations reveal that when a force pulls the N terminus of the hexameric ring, the pulling creates a torque that influences the rotation of the ring about the stalk in the *z* axis in Fig. 1*A*. The moment arm, which is measured from the line of the force to the rotational axis in the simulations, is useful in developing a phenomenological model for analytical calculations that quantitatively captures the differential detachment rates of the two heads. Our combined effort of computer modeling, simulations, and analytical calculations provides a molecular basis to explain the regulation mechanism of the interhead tension in cytoplasmic dynein.

Results

Kinetic Pathways of the Conformational Change in Cytoplasmic Dynein. In our study, the cytoplasmic dynein molecule was approximated as a ring of six AAA+ domains on the top (Fig. 1*C*, blue), a coiled-coil stalk in the middle (Fig. 1*C*, pink), and an MTBD at the bottom (Fig. 1*C*, green). For the stalk, two conformations, named the α and β registry, were observed in previous experiments (30). In the following, if the stalk is in the α registry, we will denote that the dynein in the α state; otherwise, it is in the β state. Our hypothesis is that the transition between the α and the β states might be crucial for the coordination between the two heads of cytoplasmic dynein. Therefore, to test this idea, we built a dual-basin SBM (details are given in *SI Appendix*) to monitor the transition from the α to the β state kinetically. An ensemble of 250 unbiased trajectories is presented in Fig. 2*A*, and a typical trajectory is shown in Fig. 2*B*. We employ a reaction coordinate, Q, which measures the fraction of the native contact formations of the corresponding crystal structures (see detailed definitions in Fig. 2).

The dominant kinetic path was identified as follows. The system begins with the α state, which has a low Q_{stalk} (0.2, Fig. 2*B*, pink) and low Q_{MTBD} (0.5, Fig. 2*B*, green). Then, Q_{stalk} grows from 0.2 to 0.7, indicating a gradual transition from the α to the β state. However, in this intermediated state, Q_{MTBD} still remains low (0.5). After the Q_{stalk} increase continues from 0.7 to 0.8, Q_{MTBD} increases from 0.5 to 0.9. The system now turns into the β state. Our simulation suggests a sequential conformational change propagating from the stalk to the MTBD.

Stalk Conformation Influences Cytoplasmic Dynein Binding to MT. Our computer simulation indicated that the conformation of the stalk influences the strength of the dynein binding to the MT. Since the crystal structures are not available, we have utilized a pseudoatomic model based on the cryo-EM map (21) to compute $Q_{Dynein\text{-}MT}$. It is a strong-binding state corresponding to the α state. We have chosen $Q^{\alpha}_{Dynein-MT}$ as a reaction coordinate since it is directly connected to our structure-based Hamiltonian. In the α state, the MTBD of dynein tightly binds to the MT, indicated by a high fraction of the native contact formation in the

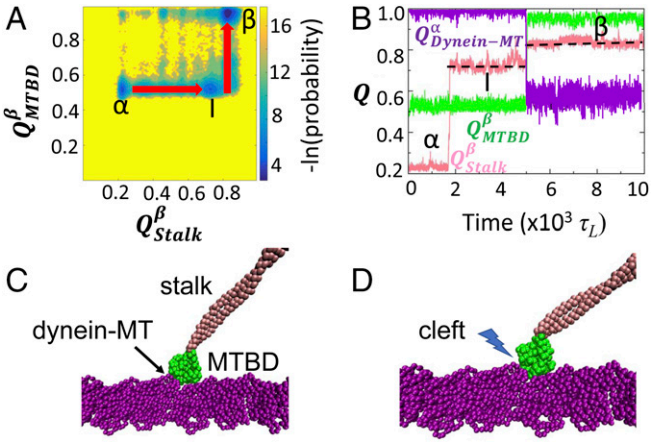

Fig. 2. Kinetic simulations of a cytoplasmic dynein changing from the α state to the β state. (*A*) Kinetic probability distribution produced from 250 unbiased kinetic trajectories from the α to the β state. The unit of the probability distribution is k_BT. Q^n_m measures the fraction of the native contact formations for a particular segment m (m = stalk, MTBD, or dynein–MT) in the n ($n = \alpha$ or β) state. The red arrow shows the dominant kinetic path. (*B*) A typical kinetic trajectory from the α to the β state. The pink line represents Q for the stalk. The green line represents Q for the MTBD. The purple line represents the fraction of the native contact formations between the MTBD and the MT when the dynein is in the α state. (*C*) Representative snapshot of the α state. The MTBD tightly binds to the MT. (*D*) Representative snapshot of the β state. The MTBD partially detaches from the MT. The cleft between the MTBD and the MT is marked with a blue arrow. The time unit is τ_L, used in our coarse-grained simulations.

dynein–MT interface, $Q_{Dynein\text{-}MT}$ (purple line in Fig. 2*B* and Fig. 2*C*). When the MTBD changes from the α state to the β state, the dynein–MT interfacial contacts in the α state cannot be simultaneously formed anymore. Subsequently, in the β state $Q^{\alpha}_{Dynein-MT}$ reduces by half (Fig. 2*B*, purple), as evident from a cleft between the dynein and the MT (Fig. 2*D*). This cleft in the β state is the consequence of conformational change of the dynein molecule itself. The loss of these contacts reduces MT binding affinity. We suggest that a reduction in the fraction of the native contact formation leads to a decrease in the binding affinity, consistent with previous experimental observations (22, 30) finding that the β state corresponds to a weaker binding state compared with the α state.

Inspired by this result, we hypothesize that for the trailing head the interhead tension will favor the transition from the α state to the β state, while for the leading head the tension will inhibit the transition. Because the β state corresponds to a weaker binding state to the MT than the α state, the trailing head will on average detach from the MT before the leading head. We will show the details of our calculations below.

Dynein Rotates About Its Stalk During the Transition from the α to the β State. Our computer simulations indicate that dynein's head rotates about its stalk during the transition from the α to the β state. Fig. 3 demonstrates the rotation, using the AAA ring as an example (the stalk also rotates). The rotation is quantified by the angle between the normal vector of the AAA ring and the main axis of the MT. The free energy basin on the left in Fig. 3 represents the α state, which has a low Q_{stalk} (0.2) as detailed above. The angle in this basin is ∼150°, indicating that the normal vector of the AAA ring and the main axis of MT are almost antiparallel. In contrast, when dynein switches to the β state (Fig. 3, the basin on the right), this angle decreases to 75°, indicating that the normal vector of the AAA ring and the main axis of MT are almost perpendicular. Thus, the conformational change between the α and the β state is associated with a rotation of the dynein molecule by 75°.

Dynein Controls Its Two Heads by the Interhead Tension. We hypothesize that the transition time of dynein from the α to the β state increases with an exerting force pointing to the plus end of the MT and decreases with an exerting force pointing to the minus end of the MT. To test this idea, we applied a force to the N terminus of the AAA ring pointing to the plus end of the MT, mimicking the case of the leading head of dynein (Fig. 4*B*), and a force pointing to the minus end of the MT, mimicking the case of the trailing head (Fig. 4*C*). Because the two forces point in opposite directions, the two corresponding torques have opposite effects. For the leading head the torque inhibits the rotation, while for the trailing head the torque favors the rotation. Indeed, in the absence of forces, the head rotates by 75° (Figs. 3 and 4*A*; the angle decreases from 150 to 75°). In contrast, with the torque, the leading head rotates only 50° (Fig. 4*B*; the angle changes from 150 to 100°) while the trailing head rotates up to 100° (Fig. 4*C*; the angle changes from 150 to 50°). Importantly, the averaged transition time from the α state to the β state, T_{tr}, is affected. The transition time for the trailing head is two times shorter than that for the leading head (Fig. 4 *B* and *C*). Our simulations therefore indicate that the trailing head reaches the β state (the weaker binding state) before the leading head does; thus, the trailing head is released from the MT earlier than the leading head. Noticeably, due to the usage of the coarse-grained model, T_{tr} measured from simulations is only used to qualitatively describe the transition time. Quantitatively, a more accurate estimation is performed by analytical modeling in the next section, which indicates that, at a force of 2 pN, T_{tr} for the trailing head is 10 times shorter than that for the leading head. In addition, we have assumed the force to be horizontal as in the experiments (16, 17). We have also explored additional force directions (*SI Appendix*, Fig. S2) and noticed that, as long as they are pointing to the plus end of the MT, the transition time of dynein from the α to the β state increases. This increase is smaller for larger angles between the force and the *x* axis.

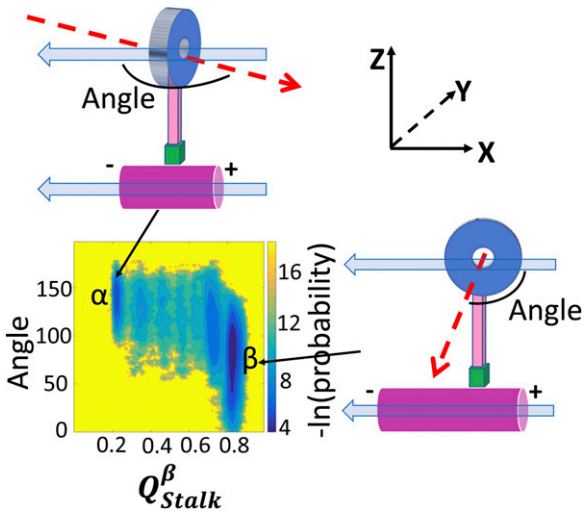

Fig. 3. Kinetic probability distribution produced by an ensemble of 250 unbiased kinetic simulations from the α to the β state, as a function of Q_{stalk} and the angle between the normal vector of the AAA ring (red dashed arrow) and the main axis of the MT (blue arrow). The unit of the probability distribution is k_BT. The AAA ring is illustrated as a blue disk with a hole in the center.

To further demonstrate the importance of the rotation for the structural transition from the α state to the β state, we designed two new simulations in addition to the former case as the control. First, we kept the force unchanged but added an energy term to the Hamiltonian to inhibit the rotation (details are given in *SI Appendix*). If the rotation is essential for the transition, inhibiting the rotation will significantly increase the transition time compared with the time in the case with uninhibited rotation (Fig. 5*A*). If the rotation is not important for the transition, the transition time should remain unchanged. Our results indeed show a threefold increase in the transition time after the rotation is inhibited (Fig. 5*B*). Second, we removed the tension but added a torsional energy term to the Hamiltonian (Fig. 5*C*) to accelerate the rotation. We observed that the transition time decreased by half compared with that of the control (Fig. 5*A*). These results strongly supported the idea that the interhead tension regulates the transition from the α to the β state by modulating the rotation of dynein.

Analytical Model for the Detachment Rates of Cytoplasmic Dynein from MT. To quantitatively understand the detachment rate of the cytoplasmic dynein from an MT, we develop a simple phenomenological model of the detachment process that can be explicitly solved. It is assumed that the dynein motor head can be found in only one of two states: the α state or the β state. Then, the overall detachment rate δ can be written as the weighted sum of being in the α state and in the β state. Each term is weighted by the probability of the corresponding conformation:

$$\delta(F) = p_{\alpha}(F)\delta_{\alpha}(F) + p_{\beta}(F)\delta_{\beta}(F), \quad [1]$$

where p_{α} and p_{β} are the stationary probabilities of state α and state β, respectively.

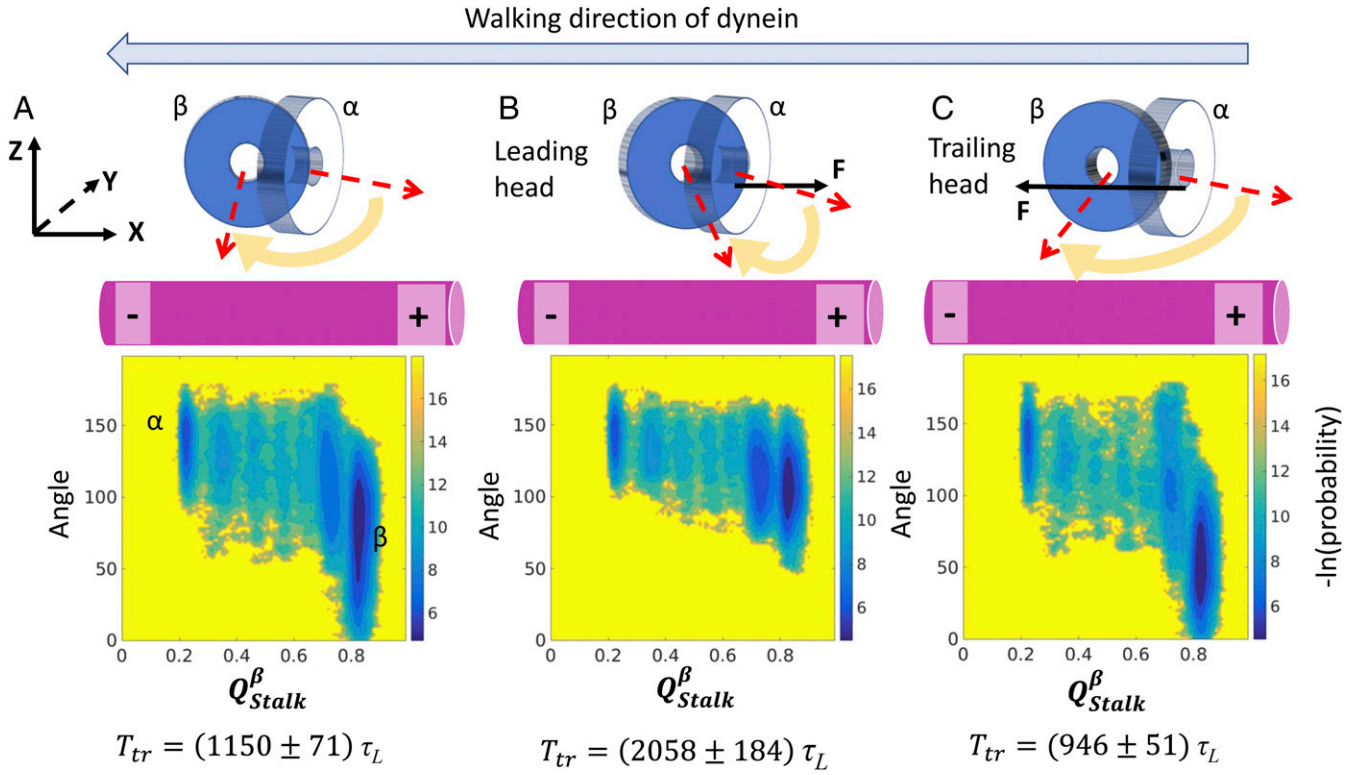

Fig. 4. Kinetic simulations of a cytoplasmic dynein during the transition from the α to the β state influenced by the interhead tension F. (*A*–*C*) Kinetic probability distribution produced from 250 unbiased kinetic simulations from the α to the β state: (*A*) F = 0, the same as Fig. 3; (*B*) F = 2 pN pointing to the plus end of the MT, mimicking the leading head; and (*C*) F = −2 pN point to the minus end of the MT, mimicking the trailing head. The *x* and *y* axes follow the definitions in Fig. 3. The red arrows represent the normal vector of the AAA ring. The blue arrow represents the walking direction of the dynein. The gold arrows represent the rotation from the α to the β state. We show the AAA ring for visualization only. For each case, the average transition time from the α to the β state, T_{tr}, is represented by error bars. τ_L is the time unit used in our coarse-grained simulations.

The interhead tension has two effects on the system. First, this tension increases the detachment rate of the α and β states (31) according to

$$\delta_{\alpha,\beta}(F) = \delta_{\alpha,\beta}(0) \times e^{\frac{Fd}{k_B T}}, \quad [2]$$

where d is an empirical parameter with a dimension of size. Its physical meaning is the distance at which the motor head should be separated from the MT to be considered dissociated. Second, this tension influences the probability of conformation in the α or the β state. Without tension, the ratio between the probabilities of the two states is determined by the free energy ΔG:

$$\frac{p_\alpha(0)}{p_\beta(0)} = e^{\Delta G/k_B T}. \quad [3]$$

However, in the presence of tension, the ratio changes due to the work performed by the torques on the motor heads, yielding

$$\frac{p_\alpha(F)}{p_\beta(F)} = e^{\frac{\Delta G}{k_B T} + \int_0^{\pi/2} F^* \frac{s^* \sin\theta}{k_B T} d\theta}, \quad [4]$$

where s is the displacement of the N terminus of AAA ring after the rotation projected to the main axis of the MT (Fig. 6*A*). This displacement is equal to 2.5 nm as determined in our simulations. $s^*\sin\theta$ is the momentum arm measured from the axis while θ is the rotation angle (Fig. 6*A*). The overall detachment rate as a function of the interhead tension can be obtained by solving coupled Eqs. **1**–**4**. Previous experiments estimated that the MT binding affinity of the α state is at least one order of magnitude larger than that of the β state (30). To simplify the calculation, we assume that $\delta_\beta(0) = 20^*\delta_\alpha(0)$. Therefore, we have three free parameters that can be varied: d, $\delta_\alpha(0)$, and ΔG. One result obtained by utilizing the parameter set d = 1.0 nm, $\delta_\alpha(0)$ = 0.2/s, and $e^{-\Delta G/k_B T} = 0.2$ is presented in Fig. 6*B*. Our results show that for the trailing head (tension > 0 in Fig. 6*B*), the detachment rate increases with the tension, while for the leading head (tension < 0 in Fig. 6*B*) the rate is insensitive to the tension. We were able to semiquantitatively reproduce previous experimental data (16, 17), which further supports our main conclusion. We estimated that for a force of 2 pN, the ratio between the transition time of the trailing head and that of the leading head is $e^{2^* \int_0^{\pi/2} F^* \frac{s^* \sin\theta}{k_B T} d\theta} = 10.8$.

Discussion

Our investigation was stimulated by previous experimental observations (7, 16, 17, 32) showing that the detachment rate of cytoplasmic dyneins from an MT in the presence of a force depends on the direction of the force. With the help of a structure-based computational model, we identified that the rotary motion of the motor heads is coupled to the conformational change from the α state to the β state. We recognize that a previous cryo-EM study (19) did not show an orientation perpendicular to MT long axis as predicted by our model. Our model shows, however, that the perpendicular state only needs to be slightly populated to be consistent with the profile of the experimental detachment rate with respect to tensions. Actually, just 5% occupation is

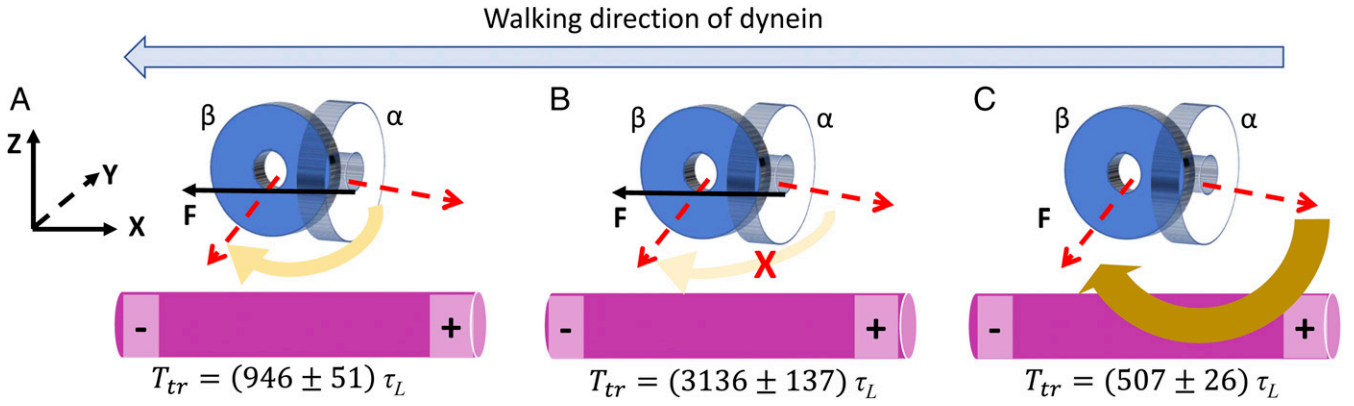

Fig. 5. Averaged time spent during the transition from the α to the β state in the simulations influenced by the rotation of dynein. (*A*) F = 2 pN, and the rotation of dynein is unperturbed (the same as Fig. 4*C*). The amplitude of the angular acceleration is presented by the size of the golden arrow. For *B* and *C*, an external torsional energy term E is added to modulate the angular acceleration (see the last paragraph in *SI Appendix*). (*B*) F = 2 pN. E is modulated so that the angular acceleration is zero (rotation of dynein is inhibited). (*C*) F = 0. E is modulated so that the angular acceleration largely increases. We show the AAA ring for visualization only. For each case, the average transition time from the α to the β state, T_{tr}, is represented by error bars. τ_L is the time unit used in our coarse-grained simulations.

sufficient (*SI Appendix*, Fig. S1). This state is probably an excited state and may therefore be difficult to be observed experimentally.

Although our simulations focused on a single motor head in the presence of forces, we inferred that a dimeric cytoplasmic dynein coordinates its two motor heads as follows (Fig. 6*C*). The interhead tension creates opposing torques that break the symmetry in the dynamic behavior of two heads. For the trailing head, the rotation is accelerated by the tension so that the transition rate from the α state (strong binding to the MT) to the β state (weak binding to the MT) increases. This change guarantees that on average the trailing head detaches from the MT before the leading head. For the leading head, the rotation is inhibited by the tension. Therefore, the leading head tends to remain in the α state (strong binding to the MT). This situation allows the leading head to attach to the MT stably when the trailing head steps forward.

Previous studies (8, 19) suggested that interhead tension can influence the interhead coordination by changing the angle between the stalk and the MT. We measured this angle in simulations. Without force, this angle is 44°. With a force pointing to the plus end of the MT, which mimics the force on the leading head, this angle decreases to 35°, while with a force pointing to the minus end of the MT, which mimics the force on the trailing head, this angle increases to 71°. Therefore, our coarse-grained model qualitatively reproduced the trend observed in a previous experiment (19) showing that interhead tension decreases the angle of the leading head and increases the angle of the trailing head.

One might assume that for the trailing head, increasing the angle between its stalk and MT will decrease the transition time T_{tr} from the α to the β state. Therefore, it is vital to determine whether the change in the stalk angle or the rotary motion of dynein is the major factor influencing the stalk registry. We explore this matter in Fig. 5. In Fig. 5*B*, we added an external force but inhibited the rotation. In this case the angle between the stalk and MT increased from 44 to 90° by the force. The transition time T_{tr} should decrease if the dominant cause is the stalk angle. The opposite takes place: T_{tr} significantly increases in the simulation (Fig. 5*B* vs. Fig. 4*A*). In Fig. 5*C* the external force is removed but the angular acceleration of the rotation is increased, causing a decrease of T_{tr} (Fig. 5*C* vs. Fig. 4*A*). In this case, the angle between the stalk and the MT under these two cases does not change (45° vs. 44°). Therefore, the faster transition likely arises from the accelerated rotations. Due to the usage of a coarse-grained model, we cannot completely exclude the possibility that the interhead tension could also coordinate the two heads by changing the angle between the stalk and the MT (8, 19) or by changing the direction in which the stalk bends (18). Nevertheless, these results strongly suggest that the rotation of dynein seems a probable mechanism that should be tested by experiments.

The rotation of the AAA ring is caused by a rotary motion between the coils of the stalk when the stalk switches between the α and the β registries. The existence of the AAA ring is not mandatory for the coordination between the two motor heads because the interhead tension can still create torque through rotation of the stalk. This result is consistent with a previous experimental finding showing that the coordination between the two heads still exists in a dynein construct without the AAA ring (16). Similar rotary motion has been observed for other motor proteins as well. Kinesin-1 has been observed to rotate under saturated ATP concentrations, which produces significant torques (33, 34). It would be interesting to study whether the rotary motion is a common feature of the regulation mechanisms in

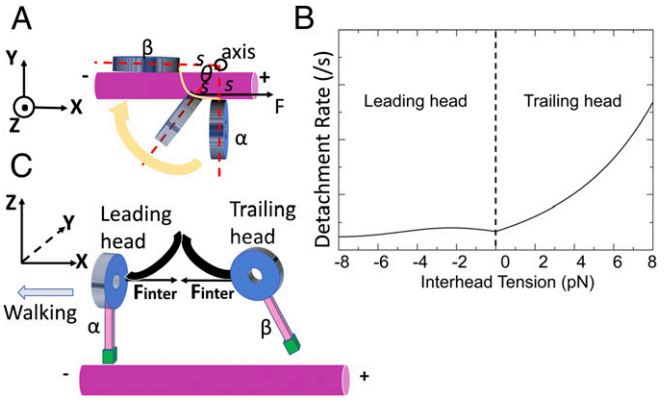

Fig. 6. Phenomenological model to understand the interhead coordination of cytoplasmic dyneins. (*A*) Illustration of the rotation of a motor head (top view). (*B*) Analytical result of the detachment rate of a motor head from an MT as a function of interhead tension. For the trailing head, the tension is larger than zero (forward). For the leading head, the tension is less than zero (backward). Previous experimental data can be found in ref. 16. (*C*) Our model for understanding the interhead coordination of a dimeric cytoplasmic dynein. The AAA ring is colored blue. The stalk is colored pink. The MTBD is colored green.

motor proteins. In addition, since we believe that the interhead tension regulates the detachment rate of dynein by regulating the transition from the α to the β state, we emphasize here that any other factors influencing the transition can also regulate the detachment rate of dynein. This influence can be achieved through an allosteric communication within the AAA rings in an ATP binding cycle (35). It can also be modified by mutations on the stalk. Indeed, the coordination between the two heads disappears upon either prevention of the relative motion between the coils of the stalk or deletion of the structural segment named the strut that connects the stalk and the AAA ring (32).

The rotary motion proposed in this work might influence the motion of dynein in additional aspects besides regulating the detachment rate of dynein. The crystal structure of human cytoplasmic dynein-2 (22) suggested that there is a coupling between the bent structure of the linker domain and the β state of the stalk. As detailed above, the interhead tension increases the probability of the β state for the trailing head. It might contribute to the conformational change of its linker domain from straight to bent (the prepowerstroke state).

The motility of cytoplasmic dyneins is a multifaceted property. In addition to the interhead coordination, several other factors are important for the motility. For example, dynactin (36) is one of the protein molecules that activate dyneins' processivity in the cellular transport. A recent experiment from Carter and coworkers (37) pointed out that dynactin influences dynein stepping by reorienting the motor domains to interact correctly with MT. This new development provides an essential insight into our next theoretical studies of dynein motor proteins that will involve dynactin as well as cargo adaptor proteins (38).

Methods

We used the C_α-only SBM (39) to represent a single head of a cytoplasmic dynein bound to an MT fragment of 16-nm length. The Hamiltonian of the system follows a previous developed self-organized polymer model (27, 29) with several modifications. The details of the Hamiltonian can be found in *SI Appendix*. The model was created by using the web server SMOG (40). A force of 2 pN was exerted on the N terminus of the AAA ring to mimic an interhead tension. For the trailing head, the exerted force pointed to the minus end of the MT. For the leading head, the exerted force pointed to the plus end.

We used the Langevin equations of motion for the coarse-grained molecular simulations. An in-house version of Gromacs 4.5 was developed (40, 41), where the nonbonded interactions was represented by a Gaussian formula (42). The Langevin equations of motion were integrated in the low friction limit with a damping coefficient of 1.0 τ_L^{-1} (43). The integration time step is $10^{-3}\tau_L$, where $\tau_L = (m\sigma^2/\varepsilon)^{0.5}$. m is the mass of a C_α bead. ε is the solvent-mediated interaction. σ is the van der Waals radius of a C_α bead. For each condition, 250 unbiased kinetic simulations were performed. Each simulation last 10^7 steps, which guaranteed a successful transition from the α to the β state. Data from all trajectories were collected and analyzed. Observables (Figs. 2*A*, 3, and 4) were expressed as $G = -k_B T \ln P$, while P was the probability collected from in the raw data. G is named the "kinetic probability distribution," a quantity used in previous work (44, 45).

ACKNOWLEDGMENTS. Work at the Center for Theoretical Biological Physics was supported by National Science Foundation Grants PHY-1427654 and MCB-1241332.

1. Kolomeisky AB (2015) *Motor Proteins and Molecular Motors* (CRC, Boca Raton, FL).
2. Alberts B, et al. (2014) *Biology of the Cell* (Garland, New York), 6th Ed.
3. Lodish H, et al. (2007) *Molecular Cell Biology* (Freeman, New York), 6th Ed.
4. Vallee RB, Williams JC, Varma D, Barnhart LE (2004) Dynein: An ancient motor protein involved in multiple modes of transport. *J Neurobiol* 58:189–200.
5. Allan VJ (2011) Cytoplasmic dynein. *Biochem Soc Trans* 39:1169–1178.
6. Reck-Peterson SL, et al. (2006) Single-molecule analysis of dynein processivity and stepping behavior. *Cell* 126:335–348.
7. Gennerich A, Carter AP, Reck-Peterson SL, Vale RD (2007) Force-induced bidirectional stepping of cytoplasmic dynein. *Cell* 131:952–965.
8. Bhabha G, Johnson GT, Schroeder CM, Vale RD (2016) How dynein moves along microtubules. *Trends Biochem Sci* 41:94–105.
9. Wang W, Cao L, Wang C, Gigant B, Knossow M (2015) Kinesin, 30 years later: Recent insights from structural studies. *Protein Sci* 24:1047–1056.
10. Trybus KM (2008) Myosin V from head to tail. *Cell Mol Life Sci* 65:1378–1389.
11. Asbury CL (2005) Kinesin: World's tiniest biped. *Curr Opin Cell Biol* 17:89–97.
12. Yildiz A, et al. (2003) Myosin V walks hand-over-hand: Single fluorophore imaging with 1.5-nm localization. *Science* 300:2061–2065.
13. DeWitt MA, Chang AY, Combs PA, Yildiz A (2012) Cytoplasmic dynein moves through uncoordinated stepping of the AAA+ ring domains. *Science* 335:221–225.
14. Qiu W, et al. (2012) Dynein achieves processive motion using both stochastic and coordinated stepping. *Nat Struct Mol Biol* 19:193–200.
15. Šarlah A, Vilfan A (2014) The winch model can explain both coordinated and uncoordinated stepping of cytoplasmic dynein. *Biophys J* 107:662–671.
16. Cleary FB, et al. (2014) Tension on the linker gates the ATP-dependent release of dynein from microtubules. *Nat Commun* 5:4587.
17. Nicholas MP, et al. (2015) Cytoplasmic dynein regulates its attachment to microtubules via nucleotide state-switched mechanosensing at multiple AAA domains. *Proc Natl Acad Sci USA* 112:6371–6376.
18. Lippert LG, et al. (2017) Angular measurements of the dynein ring reveal a stepping mechanism dependent on a flexible stalk. *Proc Natl Acad Sci USA* 114:E4564–E4573.
19. Imai H, et al. (2015) Direct observation shows superposition and large scale flexibility within cytoplasmic dynein motors moving along microtubules. *Nat Commun* 6:8179.
20. Nishikawa Y, et al. (2014) Structure of the entire stalk region of the dynein motor domain. *J Mol Biol* 426:3232–3245.
21. Redwine WB, et al. (2012) Structural basis for microtubule binding and release by dynein. *Science* 337:1532–1536.
22. Schmidt H, Zalyte R, Urnavicius L, Carter AP (2015) Structure of human cytoplasmic dynein-2 primed for its power stroke. *Nature* 518:435–438.
23. Schmidt H, Gleave ES, Carter AP (2012) Insights into dynein motor domain function from a 3.3-Å crystal structure. *Nat Struct Mol Biol* 19:492–497, S1.
24. Kon T, et al. (2012) The 2.8 Å crystal structure of the dynein motor domain. *Nature* 484:345–350.
25. Onuchic JN, Luthey-Schulten Z, Wolynes PG (1997) Theory of protein folding: The energy landscape perspective. *Annu Rev Phys Chem* 48:545–600.
26. Hyeon C, Onuchic JN (2007) Internal strain regulates the nucleotide binding site of the kinesin leading head. *Proc Natl Acad Sci USA* 104:2175–2180.
27. Zhang Z, Thirumalai D (2012) Dissecting the kinematics of the kinesin step. *Structure* 20:628–640.
28. Dutta M, Jana B (2016) Exploring the mechanochemical cycle of dynein motor proteins: Structural evidence of crucial intermediates. *Phys Chem Chem Phys* 18: 33085–33093.
29. Wang Q, et al. (2017) Molecular origin of the weak susceptibility of kinesin velocity to loads and its relation to the collective behavior of kinesins. *Proc Natl Acad Sci USA* 114:E8611–E8617.
30. Gibbons IR, et al. (2005) The affinity of the dynein microtubule-binding domain is modulated by the conformation of its coiled-coil stalk. *J Biol Chem* 280:23960–23965.
31. Fisher ME, Kolomeisky AB (2001) Simple mechanochemistry describes the dynamics of kinesin molecules. *Proc Natl Acad Sci USA* 98:7748–7753.
32. Rao L, Berger F, Nicholas MP, Gennerich A (2017) Dynein's direction-dependent microtubule-binding strength is controlled via a tension-induced sliding of Dynein's stalk helices mediated by the coiled-coil strut. *Biophys J* 112:5A.
33. Gutiérrez-Medina B, Fehr AN, Block SM (2009) Direct measurements of kinesin torsional properties reveal flexible domains and occasional stalk reversals during stepping. *Proc Natl Acad Sci USA* 106:17007–17012.
34. Ramaiya A, Roy B, Bugiel M, Schäffer E (2017) Kinesin rotates unidirectionally and generates torque while walking on microtubules. *Proc Natl Acad Sci USA* 114: 10894–10899.
35. Bhabha G, et al. (2014) Allosteric communication in the dynein motor domain. *Cell* 159:857–868.
36. King SJ, Schroer TA (2000) Dynactin increases the processivity of the cytoplasmic dynein motor. *Nat Cell Biol* 2:20–24.
37. Zhang K, et al. (2017) Cryo-EM reveals how human cytoplasmic dynein is auto-inhibited and activated. *Cell* 169:1303–1314.e18.
38. Schroeder CM, Vale RD (2016) Assembly and activation of dynein-dynactin by the cargo adaptor protein Hook3. *J Cell Biol* 214:309–318.
39. Clementi C, Nymeyer H, Onuchic JN (2000) Topological and energetic factors: What determines the structural details of the transition state ensemble and "en-route" intermediates for protein folding? An investigation for small globular proteins. *J Mol Biol* 298:937–953.
40. Noel JK, Whitford PC, Sanbonmatsu KY, Onuchic JN (2010) SMOG@ctbp: Simplified deployment of structure-based models in GROMACS. *Nucleic Acids Res* 38: W657–W661.
41. Van Der Spoel D, et al. (2005) GROMACS: Fast, flexible, and free. *J Comput Chem* 26: 1701–1718.
42. Lammert H, Schug A, Onuchic JN (2009) Robustness and generalization of structure-based models for protein folding and function. *Proteins* 77:881–891.
43. Veitshans T, Klimov D, Thirumalai D (1997) Protein folding kinetics: Timescales, pathways and energy landscapes in terms of sequence-dependent properties. *Fold Des* 2:1–22.
44. Wang Q, et al. (2013) Protein recognition and selection through conformational and mutually induced fit. *Proc Natl Acad Sci USA* 110:20545–20550.
45. Lin X, et al. (2014) Order and disorder control the functional rearrangement of influenza hemagglutinin. *Proc Natl Acad Sci USA* 111:12049–12054.